Title
MASS TRANSFER DURING SHORT SURFACE EXPOSURES IN COUNTERCURRENT FLOW

Author
King, C. Judson.

Publication Date
1964

UCRL-11196

University of California

Ernest O. Lawrence Radiation Laboratory

MASS TRANSFER DURING SHORT SURFACE EXPOSURES IN COUNTERCURRENT FLOW

Berkeley, California

DISCLAIMER

Special

UCRL-11196

UNIVERSITY OF CALIFORNIA

Lawrence Radiation Laboratory
Berkeley, California

AEC Contract No. W-7405-eng-48

MASS TRANSFER DURING SHORT SURFACE EXPOSURES IN COUNTERCURRENT FLOW

C. Judson King

January 1964

MASS TRANSFER DURING SHORT SURFACE EXPOSURES IN COUNTERCURRENT FLOW*

C. Judson King

Lawrence Radiation Laboratory and Department of Chemical Engineering
University of California
Berkeley, California

January, 1964

ABSTRACT

Numerical solutions have been obtained for mass transfer behavior during countercurrent flow of two fluid phases across a short contact interval fixed in space. Two simplified models were considered: Model 1 postulates a simple penetration behavior for both phases, whereas Model 2 postulates a laminar boundary layer behavior for one phase and a simple penetration model for the other.

Results show that the overall rate of mass transfer for these models is higher than that predicted by the classical two-film addition of resistances equation, the maximum deviation being +20% for Model 1 and +14% for Model 2.

INTRODUCTION

Applications of mass transfer between fluid phases in countercurrent flow are extremely common in practice, yet fundamental analysis of the transport process occurring in such situations is difficult and has received little attention. Except for rudimentary two-film theory, all basic models of mass transfer across a fluid interface consider only one phase at a time, usually under the assumption of a constant surface concentration. Combination of individual phase coefficients predicted in this manner without considering the interaction between the phases is in general not reliable.[6]

In essentially all practical fluid-fluid mass transfer processes the mass transfer coefficient for either or both phases can logically be expected to vary with surface position and with the age of the surface since its formation. Such is the picture presented by the penetration or surface-renewal theories and by laminar and turbulent boundary layer theories. If the mass transfer coefficient for either phase varies and the flow patterns are not perfectly matched so as to provide a constant ratio of mass transfer coefficients at all points of interface, the surface concentrations must also vary even though the bulk compositions of both phases remain constant.

Of particular concern for the design or analysis of processing equipment is the concept of the addition of individual phase mass transfer coefficients, each measured in the absence or suppression of resistance in the other phase. This is usually accomplished through use of the equation:

$$\frac{1}{K_1} = \frac{1}{k_1^*} + \frac{m}{k_2^*} \qquad (1)$$

where K_1 is the overall mass transfer coefficient based on a driving force of bulk Phase 1 concentration minus that in equilibrium with the bulk Phase 2 concentration, k_1^* and k_2^* are individual mass transfer coefficients for either phase measured in the absence or suppression of resistance in the other phase, and m is the slope of the linearized equilibrium curve

$$C_{1e} = mC_2 + b \qquad (2)$$

As has been shown elsewhere,[6] two of the restrictions necessary for this equation to hold true over a finite interfacial area are the following:

1). There must be no interaction between the individual phase coefficients; i.e., k_1 at any point must be independent of the magnitude of k_2, and vice versa.

2). The ratio (mk_1/k_2) must be constant at all points of interface.

It has also been shown that deviations from Eq. (1) may be approached by considering the separate effects of deviations occurring within single surface exposures and deviations caused by combining all surface exposures into a single, overall apparent coefficient. The remainder of this report is concerned with the effects occurring within a single surface exposure.

Cocurrent Flow

Figure 1a depicts a simple cocurrent surface exposure of two fluid phases across an interface fixed in space. A case equivalent to the application of the penetration model to both phases (laminar flow with the neglect of velocity gradients near the interface if the bulk velocities are different) has been solved by Marshall and Pigford;[9] while the case of laminar boundary layers within both phases (allowance for the velocity gradients) has been

solved by Potter.[11] In both instances the surface concentrations remain constant along the exposure interval as long as a straight-line equilibrium relationship is obeyed. The individual mass transfer coefficients are consequently the same for each phase as when determined in the absence of mass transfer resistance in the other phase, and Eq. (1) is obeyed exactly. These are instances when the flow configurations are perfectly matched so as to produce a constant ratio mk_1/k_2 at all point of interface.

In the general case of arbitrary flow models for transient mass transfer in cocurrent flow, the surface concentration gradient or individual mass transfer coefficient for each phase at a point of interface will be a function of surface concentrations at earlier surface ages, or at points of interface farther to the left in Fig. 1a. A prediction of the overall mass transfer behavior can then, in principle, be obtained by means of an iterative numerical solution of the appropriate differential equations, proceeding from the left of the diagram to the right. In any event the surface concentrations should not vary widely since the individual mass transfer coefficients should both be decreasing functions of surface age. Consequently Eq. (1) should be closely obeyed.

Countercurrent Flow

The countercurrent flow situation presented in Fig. 1b cannot be analyzed in as ready a fashion as the cocurrent flow case. In the first place, the surface concentrations cannot be expected to be constant along the interval since the surface concentration of Phase 1 should be that of the bulk of Phase 1 at the right and in equilibrium with the bulk of Phase 2 at the left. Second, since the surface concentration gradient within either phase at a point of interface is a function of surface conditions at earlier

ages, the gradient in Phase 1 will be dependent upon behavior to the right of the point while the gradient in Phase 2 will be dependent upon behavior to the left of the point. A simple iterative solution from one end of the interface to the other is no longer possible, and instead the surface conditions of the entire exposure interval must be known or assumed in order to predict the mass flux across the interface at any point.

As a result of this added complexity, no mass transfer solutions have been reported for cases of countercurrent flow where transient effects must be considered in both phases. On the other hand, several authors have solved the case of a penetration model for one phase in contact with a simple film model for the second phase.[3,8,10,12] The result is obtained analytically, since the transient nature of the second phase has been removed and the surface boundary condition for the first phase has been changed in a readily definable way from that of a constant surface concentration to a flux specification in terms of the surface concentration. The results of this solution show a maximum deviation from Eq. (1) of 5% (see Fig. 2), with the true K_1 always being greater than that predicted from Eq. (1).

If no slip is allowed between the phases at the interface, another complicating factor is introduced. The interface will in general have a finite velocity in one direction or the other. Solutions for single phase mass transfer have been reported for cases where the interface moves in the same direction as the bulk phase,[1] but the case where the interface moves in the opposite direction from the bulk phase is more difficult to analyze. The flow will reverse direction at some point within the phase away from the interface, thus making analytical or numerical solution cumbersome.

FLOW MODELS

Two countercurrent flow models were examined in this study. They were chosen by two main criteria -- to provide limits upon the deviations from Eq. (1) in realistic flow situations, and to be susceptible to numerical mathematical analysis without the consumption of a large amount of digital computer time. Only cases of low net rates of mass transfer have been considered.

Model 1 pictures non-viscous countercurrent flow. A simple penetration model is obeyed by both phases, with no gradients of velocity within either phase near the interface. The velocity at all points within each phase is the bulk velocity of that phase; there is consequently total slip at the interface. This model allows for the deepest penetration of the concentration profiles into both phases during a given exposure since the removal or supply of solute by diffusion and convection is equally effective at all points, rather than being more effective at points further from the interface as is the case for other models. The model would apply to fictitious cases of countercurrent mass transfer where the Schmidt number is substantially less than 1.0,[4] or to liquid metal heat transfer.

Model 2 approximates a laminar countercurrent contacting between a gas and a liquid. A simple penetration model is again followed by one phase (liquid), while the second phase (gas) has a locally varying velocity described by

$$u = ay/\sqrt{x} \tag{3}$$

$$v = \frac{a}{4} y^2/x^{3/2} \tag{4}$$

where u is the velocity in the X direction (parallel to the interface), v is the velocity in the y direction (normal to the interface) and $\underline{a}$ is a proportionality constant equal to $0.343\, u_B \sqrt{u/\nu}$. u_b is the bulk phase velocity away from the interface and ν is the kinematic viscosity.

Equation (3) will be recognized as the first term of the Pohlhausen approximation to the laminar boundary layer profile, and is capable of fitting the velocity closely for much of the distance into a boundary layer. Equation (4) is the consequence of continuity. Boundary layer mass transfer coefficients based upon these velocity expressions for mass transfer to a single phase equal those from more elaborate representations to within a few per cent for Schmidt numbers down to 0.5.[4]

This model postulates that the gas phase is stagnant at the interface, whereas the liquid phase possesses a finite velocity. Thus again there is slip at the interface. The solution of Beek and Bakker for interfacial motion in the direction of bulk flow[1] may be interpreted in rough fashion to indicate that the interfacial velocity must be more than 10% of the bulk gas velocity in order for the gas phase mass transfer coefficient to deviate by more than 10% from that for a stagnant interface. If this thinking may be applied to countercurrent flow, then Model 2 can be expected to fit the real countercurrent gas-liquid case reasonably well as long as the bulk liquid velocity is less than 10% of the bulk gas velocity.

MATHEMATICAL APPROACH

The transport behavior of either phase may be described by the equation

$$u \frac{\partial c}{\partial x} + v \frac{\partial c}{\partial y} = \frac{\partial^2 c}{\partial y^2} . \qquad (5)$$

For both phases in Model 1 and for Phase 1 in Model 2, u is constant at u_B and v is zero. For Phase 2 in Model 2, u and v are given by Eqs. (3) and (4). Boundary conditions include specifications that the entrance concentration and the concentrations far from the interface for either phase are fixed and equal to the bulk concentration of that phase. The interfacial concentrations of the phases at any point of interface must be in equilibrium with one another, and the interfacial flux must be the same for both phases at any point. The assumptions of a semi-infinite medium and of no change in bulk phase compositions are applicable to relatively short exposure times such as are characteristic of industrial equipment.

The solution procedure involved assuming a profile of interfacial concentrations, and then solving for the interfacial flux from each phase. The degree of mis-match of the fluxes at each point of interface was ascertained and compared to a predetermined allowable error. If the mismatch was greater than allowable, the assumed interfacial concentrations at that point were corrected in the direction indicated for a match. A convergence factor was employed which allowed the correction to be greater or less than indicated, as desired. Between 20 and 40% over-correction was found to give the most rapid, uniform convergence. The computations were carried out with the IBM 7094 digital computer of the Lawrence Radiation Laboratory.

Several methods are available for solving finite difference approximations to Eq. (4).[7] The forward difference (or explicit) scheme was employed for Model 1, after it was confirmed that the results obtained were indistinguishable from those produced by the symmetrical Crank-Nicholson implicit representation. On the other hand the more lengthy Crank-Nicholson approach was employed for Model 2 since the coefficients of the finite difference equation changed markedly from point to point in the concentration net for the phase approximating boundary layer behavior. The improved stability and convergence characteristics of the Crank-Nicholson approach were necessary to cope successfully with that situation.

The total amount of mass transfer was obtained by each of two different means -- by integrating the local fluxes at all individual points of interface across the entire interface, and by integrating the exit concentrations from both phases as a function of distance normal to the interface. For both flow models it is possible to express the deviation of the total mass transfer from that predicted by Eq. (1) as a unique function of the ratio mk_1^*/k_2^*, denoted by $\underline{R}$.

For fine enough net sizes the two methods for obtaining the total mass transfer gave equivalent results, as expected. The chief error involved in the use of the integration of the local interfacial fluxes was the fact that the flux at either end of the exposure interval became very large and provided a contribution which could be estimated only within limits. The phase presenting the greater portion of the total resistance to mass transfer gave the more accurate result upon integration of exit concentrations for determining the total mass transfer; a close approximation to the total amount of mass transfer was obtained by this method even for relatively coarse nets. In any event the use of 200 steps along the interface served to fix the total amount of mass transfer within 1%.

The finite difference modulus, β , of Reference 7 was fixed at 0.25 for all computations after initial exploratory calculations. In the case of the boundary layer approximation this condition served to maintain a positive effect of past concentrations upon future concentrations at all important points in the net.

Some computations were made with a variable net size at the extreme ends of the exposure interval. These gained little in the way of accuracy because the change in interfacial concentrations was relatively rapid at all points of interface. Computations were also made for a single phase exposure with specified surface concentrations corresponding to known analytical solutions. The results of these calculations are described in Appendix B; they served to confirm the general reliability of the method and to determine the relative merits of the methods for obtaining the total amount of mass transfer.

Details of the mathematical procedures are located in Appendix A.

COMPUTATIONAL RESULTS

The results of the computations performed for the two flow models are shown in Figs. 1-7. The deviations of the average mass transfer rates from those predicted by Eq. (1) are presented in Fig. 2 as K_1/K_{F1}, the ratio of the overall mass transfer coefficient to that predicted by Eq. (1). For comparison the result for the case of a penetration model for Phase 1 and a film model for Phase 2, previously referred to, is also included and is denoted "Model 3".

Figure 3 presents the local interfacial fluxes for Model 1 with various values of R. The case of $R = \infty$ corresponds to the penetration solution for Phase 2 with a constant interfacial concentration. The flux profiles for $R < 1$ are mirror images of the profile for the reciprocal value of R. Figure 4 compares the interfacial flux profiles for the three models in the case of $R = 1$.

The interfacial concentration profiles for Model 1 and various values of R are given in Fig. 5. For $R < 1$ the ordinate is equal to 1.0 minus the ordinate for the reciprocal value of R. In Fig. 6 the interfacial concentrations for all three modesl are compared in the instance where $R = 1$.

The effluent concentration profiles as a function of distance normal to the interface for Models 1 and 2 with $R = 1$ are presented in dimensionless form in Fig. 7 as Curves 1-3. Effluent concentration profiles are also included for the case of a single phase obeying a penetration model (Curve 4), and for a single phase obeying a film model (Curve 5). These latter curves represent solutions for a constant surface composition with a concentration driving force equal to half the driving force considered for the countercurrent models. They are included to allow comparison of relative shapes of concentration profiles.

Comparison of Models

From Curves 1 and 4 in Fig. 7 it may be seen that the effluent concentration profile is steeper near the interface for countercurrent flow Model 1 than for the single phase penetration model; the mass transfer effect has not propagated as great a distance into the fluid. This behavior stems from the fact that the change of interfacial concentration away from the bulk concentration has occurred at a greater age of the fluid in the countercurrent model. On the other hand there has been considerably more mass transfer toward the end of the exposure in the countercurrent case because of the rapidly changing surface concentration. This fact is verified by a comparison of the left hand portions of the curves for $R = 1$ and $R = \infty$ in Fig. 3.

Curves 1 and 2 in Fig. 7, representing the effluent concentrations from the phases obeying the penetration model in flow Models 1 and 2, are quite close to one another. This is the result of similar interfacial concentration profiles for the two models, as shown in Fig. 6. Curve 2 is slightly lower than Curve 1 in Fig. 7 because of the lesser total amount of mass transfer, shown in Fig. 2.

Curve 3 in Fig. 7 is steeper than Curve 2 because the boundary layer model postulates a more effective removal or supply of solute at points far from the interface than at points nearer the interface. In this respect the boundary layer model represents an intermediate case between the penetration and film models, since the film model pictures an infinite capability for solute removal or supply beyond a certain distance from the interface.

It is therefore logical that the curve for Model 2 lies below the curve for Model 1 in Fig. 2, and that the curve for Model 3 lies below that for Model 2. The three models represent differing degrees of variation from

the picture afforded by a two-film model for countercurrent flow: Equation (1) is based upon a two-film model and, therefore, is obeyed exactly for a two-film model. Model 3 retains the film behavior for one phase and thus gives less deviation than Model 1 which rejects the film model in favor of the penetration model for both phases. Model 2 employs a behavior for Phase 2 intermediate between Models 1 and 3, and thus exhibits a deviation from Eq. (1) intermediate between the deviations of Models 1 and 3.

Model 2 probably represents the upper limit for deviations from Eq. (1) in a gas-liquid countercurrent contacting where the gas phase forms both velocity and concentration boundary layers following the point of initial contact. If the liquid phase velocity across the exposure interval is large enough to necessitate consideration of an interfacial gas velocity significant in comparison to the bulk gas velocity, then the flow immediately adjacent to the interface will be cocurrent. As has been shown, cocurrent contacting of phases tends to give close agreement with Eq. (1).

Applications to Equipment

The chief value of this work lies in furthering the understanding of simple countercurrent mass transfer processes and in enabling the interpretation of data acquired in simple laboratory devices, such as the short wetted wall column, which provide a single exposure interval.

Large scale mass transfer devices, such as plate columns or packed columns, are much more complex than the simple flow models presented here. One promising approach to the analysis of such equipment, however, is to realize that they are made up of many short surface exposures. The analysis may then be broken down to a consideration of the behavior of individual exposures, followed by a consideration of the result of compounding all the individual exposures together into a single gross observation.[6]

From the present results it can be concluded that the average mass transfer coefficient for an individual countercurrent surface exposure will be higher than predicted by Eq. (1). The deviation will range from 0 to +14% depending upon the flow model and the value of R. In the fictitious case of Schmidt numbers will below 1.0 in each phase (Model 1) the deviation would be as high as +20%.

When the contributions of the individual exposures are compounded into an overall observed mass transfer coefficient, variations in the ratio mk_1^*/k_2^* from one exposure interval to another will tend to reduce the observed mass transfer coefficient as compared to that predicted by Eq. (1). The net result for packed and plate towers appears to be that the observed overall mass transfer coefficients are less than those predicted from Eq. (1). This is evidenced by the fact that coefficients for the absorption of ammonia, acetone, methanol, etc., into water are uniformly lower than those predicted by Eq. (1) from vaporization and oxygen desorption data, often by factors of 100% or more.[6] Thus the negative deviations caused by variations in mk_1^*/k_2^* from one exposure interval to another more than offset the positive deviations within each exposure interval for packed and plate columns.

APPENDICES

A. Details of Mathematical Procedure

1. Model 1.

The mass transfer coefficient for Phase 1 is given by simple penetration theory as

$$k_1^* = 2\sqrt{\frac{u_{B1} D_1}{\pi L}} , \qquad \text{(A-1)}$$

when the resistance to mass transfer in Phase 2 is absent or negligible. An analogous expression provides the coefficient for Phase 2 when there is no significant resistance in Phase 1. Consequently R , defined as mk_1^*/k_2^* , is given by

$$R = m\sqrt{\frac{u_{B1} D_1}{u_{B2} D_2}} . \qquad \text{(A-2)}$$

If the value of K_1 calculated from Eq. (1) is denoted by K_{F1} , we have

$$\frac{k_1^*}{K_{F1}} = 1 + R \qquad \text{(A-3)}$$

The object is to compute the true value of K_1 for the case where Phases 1 and 2 are brought together in a single countercurrent exposure, and then to compare that value with K_{F1} .

The transport behavior of both phases is given by the differential equation

$$D \frac{\partial^2 c}{\partial y^2} = u_B \frac{\partial c}{\partial X} , \qquad \text{(A-4)}$$

which was approximated by a finite difference representation. Both the forward-difference explicit form and the symmetrical Crank-Nicholson implicit form were employed. As is shown by Lapidus[7] a single parameter, β, is required for either approach and is an indication of the relative net sizes in the X and y directions. β was equal for the two phases; thus

$$\beta = \frac{D_1 \Delta X_1}{u_{B1}(\Delta y_1)^2} = \frac{D_2 \Delta X_2}{u_{B2}(\Delta y_2)^2} . \qquad \text{(A-5)}$$

The X direction net size was taken to be the same for both phases ($\Delta X = L/N_X$); hence

$$\frac{\Delta y_1}{\Delta y_2} = \sqrt{\frac{D_1 u_{B2}}{D_2 u_{B1}}} \qquad \text{(A-6)}$$

It was necessary to make an initial assumption for the interfacial concentration profile. This was accomplished by setting

$$C_1(X,0) = \frac{1000}{1 + R\sqrt{\frac{L-X}{X}}} \qquad \text{(A-7)}$$

and

$$\eta\, C_2(X,0) + b = C_1(L-X,0) \qquad \text{(A-8)}$$

In this way X was defined for each phase as the distance along the interface from the point of entrance of that phase; thus X in Phase 1 corresponds to $L-X$ in Phase 2, and vice versa. The bulk concentration of Phase 1 was taken as 0 and that of Phase 2 as $1000/m$ in relative units; b was taken equal to zero in Eq. (A-8).* The resulting assumed interfacial concentration profile is that which would result if k_1/k_2 were equal to k_1^*/k_2^* at all points.

The entire concentration patterns for Phase 1 (as C_1) and Phase 2 (as mC_2) were then solved in straightforward fashion following the procedures detailed by Lapidus.[7] The Thomas method was employed for solving the successive sets of simultaneous equations in the Crank-Nicholson approach.

The equality of fluxes at all points of interface was then checked. The necessary condition is

$$D_1 \left(\frac{\partial C_1}{\partial y_1}\right)_{X, y_1=0} = -D_2 \left(\frac{\partial C_2}{\partial y_2}\right)_{L-X, y_2=0} \qquad \text{(A-9)}$$

The derivatives were approximated by the five-point expression given by Hildebrand:[5]

$$\left(\frac{\partial C}{\partial y}\right)_{-2} = \frac{1}{12\Delta y} \left(-25\, C_{-2} + 48\, C_{-1} - 36\, C_0 + 16\, C_1 - 3\, C_2\right) + \frac{(\Delta y)^4}{5} \frac{\partial^5 C}{\partial y^5}(\xi) \qquad \text{(A-10)}$$

*These bases are arbitrary and supply a scaled driving force which cancels out when a mass transfer coefficient is obtained. Insertion of a finite value for b would serve merely to add a constant to all the concentrations in one phase, with no resultant effect upon fluxes or mass transfer coefficients.

Condition (A-9) then becomes

$$\mathcal{m} \cdot \left[\frac{25\ C_2(L-X,0)-48\ C_2(L-X,\Delta y_2)\ 36\ C_2(L-X,2\Delta y_2)-16\ C_2(L-X,3\Delta y_2)\ 3\ C_2(L-X,4\Delta y_2)}{-25\ C_1(X,0)+48\ C_1(X,\Delta y_1)-36\ C_1(X,2\Delta y_1)+16\ C_1(X,3\Delta y_1)-3\ C_1(X,4\Delta y_2)} \right]$$

$$= \frac{D_1}{D_2} \cdot \frac{\Delta y_2}{\Delta y_1} \cdot \mathcal{m}$$

$$= \mathcal{m} \sqrt{\frac{D_1\ u_{B1}}{D_2\ u_{B2}}}$$

$$= R \qquad \text{(A-11)}$$

To the extent that the assumed interfacial concentration profile is incorrect, this condition will not be met. The relative error

$$\left| \frac{[\text{L.H.S. Eq. (A-11)}] - R}{R} \right|$$

was compared with an allowable error. If the error at any points of interface exceeded the allowable, the assumed interfacial compositions at those points were adjusted and the entire calculation was repeated until convergence was obtained. The corrected interfacial concentrations were computed as

$$[C_1(X,0)]_{NEW} = [C_1(X,0)]_{OLD}$$

$$+ F \left\{ \frac{m[48\ C_2(L-X,\Delta y_2)-36\ C_2(L-X,2\Delta y_2) + 16\ C_2(L-X,3\Delta y_2)-3\ C_2(L-X,4\Delta y_2)]}{25\ (R+1)} \right.$$

$$+ \frac{R[48\ C_1(X,\Delta y_2)-36\ C_1(X,2\Delta y_2)+16\ C_1(X,3\Delta y_2)-3\ C_1(X,4\Delta y_2)]}{25\ (R+1)} - [C_1(X,0)_{OLD}]\Bigg\}, \quad \text{(A-12)}$$

where the convergence factor, F, lay between 1.0 and 1.5. Twenty or more trials were usually required for convergence.

The total amount of mass transfer across the interface was obtained in two different ways:

A. Integration of Fluxes at all Points of Interface. The local overall mass transfer coefficient is defined as

$$K_{1X} = \frac{\text{Flux}}{1000}$$

$$= -\frac{D_1}{1000}\left(\frac{\partial C_1}{\partial y_1}\right)_{y_1=0}, \quad \text{(A-13)}$$

since the overall concentration driving force was taken to be 1000. Making use of Eqs. (A-1), (A-3) and (A-5), Eq. (A-13) may be approximated by

$$\frac{K_{1X}}{K_{F1}} = \frac{1+R}{24{,}000}\sqrt{\pi\beta N_X}\cdot\Big[25\ C_1(X,0)-48\ C_1(X,\Delta y_1)+36\ C_1(X,2\Delta y_1) -$$

$$- 16\ C_1(X,3\Delta y_1)+3\ C_1(X,4\ y_1)\Big], \quad \text{(A-14)}$$

where $L/\Delta X$ has been replaced by N_X. The average mass transfer coefficient K_1, as compared to that predicted by Eq. (1), was then obtained by an integration,

$$\frac{K_1}{K_{F1}} = \int_{\frac{1}{N_\chi}}^{1-\frac{1}{N_\chi}} \frac{K_{1\chi}}{K_{F1}} \quad d\left(\frac{\chi}{L}\right) \tag{A-15}$$

computed by use of Simpson's rule. At either end of the exposure interval the flux becomes very large. The additional contribution of the end slices to the total mass transfer was estimated by assuming that the flux in these slices varied inversely as the square root of the distance from the closer end of the interface. The correction became small for fine net sizes.

B. Integration of Effluent Concentrations. The average effluent concentration in Phase 1 must correspond to the net amount of mass transfer:

$$1000\ K_1\ L = \int_0^\infty u_{B1}\ C_1(L,y_1)\ dy_1 \tag{A-16}$$

Combining Eq. (A-16) with Eqs. (A-1) and (A-3) gives

$$\frac{K_1}{K_{F1}} = \frac{1+R}{2000}\sqrt{\frac{\pi\ u_{B1}}{D_1\ L}} \int_0^\infty C_1(L,y_1)\ dy_1 \tag{A-17}$$

The integration was carried out by Simpson's rule, with Δy_1 being eliminated through use of Eq. (A-5):

$$\frac{K_1}{K_{F1}} = \frac{1+R}{6000}\sqrt{\frac{\pi}{\beta\ N_\chi}} \left[C_1(L,0) + 4\ C_1(L,\Delta y_1) + 2\ C_1(L,2\Delta y_1) +\right.$$

$$+ \; 4\, C_1(L,3\Delta y_1) + 2\, C_1(L,4\Delta y_1) + \ldots \Big] \qquad \text{(A-18)}$$

A similar analysis based upon the Phase 2 effluent concentrations gives

$$\frac{K_1}{K_{F1}} = \frac{1+R}{6000R}\sqrt{\frac{\pi}{\beta N_\chi}} \left\{ 1000 - mC_2(L,0) + 4\,[1000 - mC_2(L,\Delta y_2)] + \right.$$

$$\left. + 2[1000 - mC_2(L,2\Delta y_2)] + \ldots \right\} \qquad \text{(A-19)}$$

2. Model 2.

The flow behavior of Phase 1 is identical to that in Model 1; hence such characteristics as k_1^*, k_1/K_{F1}, etc., remain the same. On the other hand the flow pattern chosen for Phase 2 and described by Eqs. (3) and (4) leads to (1)

$$k_2^* = 0.684 \left(\frac{D_2^4 \, u_{B2}^3}{\nu_2 \, L^3} \right)^{1/6} \qquad \text{(A-20)}$$

Therefore

$$R = \frac{mk_1^*}{k_2^*} = 1.65\; m \left(\frac{u_{B1}^3 \, D_1^3 \, \nu_2}{D_2^4 \, u_{B2}^3} \right)^{1/6} \qquad \text{(A-21)}$$

Equation (A-4) once again describes the transport behavior of Phase 1; however, for Phase 2, Eq. (5) holds in its more general form, with u and v given by Eqs. (3) and (4).

The coefficients of Eq. (5) vary markedly with position in Phase 2; consequently the Crank-Nicholson symmetrical implicit finite difference representation was employed for both phases. β was set for Phase 1 by the left-hand equality of Eq. (A-5), thus relating Δy_1 to ΔX. By analogy to Model 1, $\Delta y_2'$ was related to Δy_1 through

$$\Delta y_2 = \frac{RD_2}{mD_1} \cdot \Delta y_1 \qquad \text{(A-22)}$$

The finite difference approximation

$$\frac{u}{\Delta X}\,[C_2(i,j)-C_2(i-1,j)]+\frac{v}{4\Delta y_2}\,[C_2(i,j+1)-C_2(i,j-1)+C_2(i-1,j+1)-C_2(i-1,j-1)] =$$

$$= \frac{D_2}{2(\Delta y)^2}\,[C_2(i,j+1)-2\,C_2(i,j)+C_2(i,j-1)+C_2(i-1,j+1) -$$

$$- \;2\,C_2(i-1,j)+C_2(i-1,j-1)] \qquad \text{(A-23)}$$

can then be transformed to

$$(\gamma-1)\,C_2(i,j+1) + (\delta+2)\,C_2(i,j) + (-\gamma-1)\,C_2(i,j-1) =$$

$$= (1-\gamma)\,C_2(i-1,j+1) + (\delta-2)\,C_2(i-1,j) + (1+\gamma)\,C_2(i-1,j-1), \qquad \text{(A-24)}$$

where γ and δ are coefficients evaluated at the X corresponding to position $i-1/2$ and the y corresponding to position j (the central point of symmetry of the computational molecule):

$$\gamma = \frac{0.192}{\beta^{3/2}} \cdot \frac{(y_2/\Delta y_2)^2}{(x/\Delta x)^{3/2}} \qquad \text{(A-25)}$$

$$\delta = \frac{3.07}{\beta^{3/2}} \cdot \frac{(y_2/\Delta y_2)}{(x/\Delta x)^{1/2}} \qquad \text{(A-26)}$$

Solution of the entire Phase 2 concentration pattern proceeded in standard fashion, using the Thomas method to solve the simultaneous equations represented by Eq. (A-24).

The convergence procedure, the flux calculations and the computation of the total mass transfer by integration of Phase 1 effluent concentrations were the same as for Model 1. The velocity gradient within Phase 2 necessitated an altered form of calculation of the total mass transfer from the effluent concentrations of Phase 2. Equation (A-16) now takes the form

$$1000\ m\ K_1 L = \int_0^\infty u_2(L,y_2)\ \ [1000-mC_2(L,y_2)]\ \ dy_2 \qquad \text{(A-27)}$$

Combination of Eq. (A-27) with Eqs. (A-3), (A-20) and (A-21) then yields

$$\frac{K_1}{K_{F1}} = \frac{1+R}{1129\ m}\sqrt{\frac{1}{u_{B1}\ D_1 L}}\int_0^\infty u_2(L,y_2)\ \ [1000-mC_2(L,y_2)]\ dy_2 \qquad \text{(A-28)}$$

Introduction of Simpson's Rule and Eqs. (2), (A-5), (A-21) and (A-22) finally yields

$$\frac{K_1}{K_{F1}} = \frac{1 + R}{2200\ R\beta N_\chi} \left\{ (1)(4)[1000\text{-}mC_2(L,\Delta y_2)] + (2)(2)[1000\text{-}mC_2(L,2\Delta y_2)] + \right.$$

$$\left. + (3)(4)[1000\text{-}mC_2(L,3\Delta y_2)] + (4)(2)[1000\text{-}mC_2(L,4\Delta y_2)] + \ldots \right\} \qquad \text{(A-29)}$$

The final programs employed for Model 1 and Model 2 computations are included as Tables 4 and 5.

B. Single Phase Calculations with Specified Interfacial Concentrations

Table 1 shows the results of a series of computations made by applying the simple penetration model to a single phase with a specified profile of interfacial concentrations. Total rates of mass transfer calculated by each of the two aforementioned methods are presented in comparison to known analytical solutions for the rate of mass transfer.[2] All rates are put on a common basis wherein the rate for a constant surface concentration of 1000 is taken as 1.000. The bulk fluid is initially solute free in all cases.

The first interfacial concentration profile represents a constant concentration and thus a mass flux which decreases as the 1/2 power of surface age. The second profile corresponds to a linearly increasing concentration, and hence a flux which increases as the 1/2 power of surface age. The third profile gives a concentration increasing as the 1/2 power of surface age, which corresponds to a constant mass flux. The fourth and fifth concentration profiles represent attempts to simulate through polynomial approximation the shapes of the concentration profiles shown in Fig. 5 for the countercurrent flow models. The program of Table 4 includes provision for these computations.

It should be noted that, in general, Method B (Integration of effluent concentrations) gives a mass transfer rate which matches the analytical solution more closely than the rate obtained by Method A (Integration of individual fluxes). This is particularly true for the two cases which simulate the countercurrent interfacial concentration profiles. On the other hand, both methods converge toward the analytical solution as the net size in the calcultation is made finer.

For the fourth and fifth profiles it was also noticed that a close approximation to the true mass transfer rate for the entire interface was given by the average of the fluxes from just the interior points of interface, neglecting the transfer in the two end slices. This amounts to considering only the mass transfer between $x/L = 1/N_x$ and $x/L = 1 - 1/N_x$. For the fourth profile the average rates obtained in this manner were 0.621, 0.624 and 0.626 for N_x = 100, 200 and 500 respectively, and for the fifth profile the average rates were 0.590, 0.596 and 0.600 for N_x = 100, 200 and 500 respectively.

Table 1. Mass Transfer Rates for Specified Interfacial Concentration Profiles - Penetration Model

β	N_χ	Average Mass Transfer Rate (Relative) Analytical Solu.	Method A*	Method B**
1. $C(X,0) = 1000$				
0.250	100	1.000	0.981	1.002
0.250	200	1.000	0.986	1.001
0.250	500	1.000	0.991	1.000
0.250	1000	1.000	0.993	0.999
0.125	100	1.000	1.010	1.003
2. $C(X,0) = (1000) \cdot (X/L)$				
0.250	100	0.667	0.667	0.666
0.250	200	0.667	0.667	0.666
0.250	500	0.667	0.667	0.666
3. $C(X,0) = (1000) \cdot (X/L)^{1/2}$				
0.250	100	0.785	0.787	0.784
0.250	200	0.785	0.787	0.785
0.250	500	0.785	0.786	0.785
4. $C(X,0) = (800) \cdot (X/L)^{1/2} - (212) \cdot (X/L)^2 + (412) \cdot (X/L)^{10}$				
0.250	100	0.627	0.679	0.625
0.250	200	0.627	0.654	0.626
0.250	500	0.627	0.638	0.626

Table 1. (cont'd)

β	N_χ	Average Mass Transfer Rate (Relative) Analytical Solu.	Method A*	Method B**
5. $C(\chi,0) = -(1111\cdot1) \cdot (\chi/L) + (1500) \cdot (\chi/L)^{1/2} + (611\cdot1) \cdot (\chi/L)^{10}$				
0.250	100	0.602	0.670	0.601
0.250	200	0.602	0.638	0.601
0.250	500	0.602	0.617	0.602

*Integration of Fluxes at all Points of Interface.

**Integration of Effluent Concentrations.

C. Tablulated Results for Countercurrent Flow Models

Model 1

Table 2 presents computational results for flow model No. 1. As was the case for Profiles No. 4 and 5 in Appendix B, there is a discrepancy among the average rates of mass transfer predicted by the various means available. As the net size is altered, the least change is noted in the rates predicted from the effluent concentrations of the phase offering the controlling resistance to mass transfer and in those rates obtained as the average of the interior interfacial points alone. This behavior is in agreement with the computations for a single phase with a specified interfacial concentration, where these two means of obtaining the mass transfer rate were found to coincide more closely with the analytical solution.

The "indicated results" in the final column are obtained primarily as extrapolations of these two means of predicting overall rates, although it should be emphasized that all four approaches converge toward the indicated accepted result.

The rate of mass transfer obtained by integration of effluent concentrations of the phase presenting the lesser portion of the total resistance is higher and less accurate than that obtained from the phase presenting the greater portion of the resistance. The cause of this phenomenon is two-fold: First, there is some displacement of the interfacial concentration profile resulting from errors in the five point approximation to the interfacial concentration gradient. This leads to a larger error in the mass transfer from the phase presenting the lesser resistance to mass transfer. Second, and most important at relatively high or relatively low values of R, there are errors in the Simpson's rule integration of the effluent concentrations.

Table 2. Computational Results for Countercurrent Flow Model No. 1

R	β	N_χ	K_1/K_{F1} Method A*	Method A**	Method B Phase 1	Method B Phase 2	Indicated Result
1	0.125	200	1.228	1.192	1.216	1.216	
1	0.250	100	1.265	1.190	1.214	1.214	
1	0.250	200	1.239	1.192	1.209	1.209	
1	0.250	400	1.223	1.195	1.205	1.205	1.198
2	0.250	100	1.248	1.156	1.231	1.168	
2	0.250	200	1.221	1.162	1.211	1.167	1.165
3	0.250	100	1.226	1.117	1.251	1.132	
3	0.250	200	1.196	1.124	1.214	1.132	1.132
5	0.250	100	1.200	1.070	1.324	1.089	
5	0.250	200	1.166	1.077	1.251	1.090	1.092
8	0.250	100	1.179	1.034	1.468	1.059	1.062
10	0.250	100	1.172	1.022	1.574	1.048	
10	0.250	200	1.136	1.030	1.414	1.049	1.051
20	0.250	100	1.155	0.994	2.139	1.024	
20	0.250	200	1.121	1.006	1.804	1.025	1.027
100	0.250	100	1.142	0.969	6.823	1.002	1.006
1000	0.250	100	1.138	0.963	59.714	0.997	1.001

*Considering mass transfer in end slices.

**Average for interior points of interface alone.

The exit interfacial concentration of Phase 1 is necessarily 1000. When R is high, all other effluent concentrations are very low compared to 1000; for example, in the case of R = 100 the concentration at the first effluent position removed from the interface is only 14.5. The result is that the Simpson integration procedure gives undue weight to the interfacial concentration of 1000 and yields an integrated effluent concentration that is too high.

Table 3 presents similar results for flow model No. 2. The values of K_1/K_{F1} reported for Method A in this instance are the average of the results obtained by the two means employed for Model 1 in Table 2. This figure is relatively insensitive to changes in net size for Model 2. The values of K_1/K_{F1} computed from the Phase 2 effluent concentrations are less accurate for Model 2 than for Model 1 because of the higher weight accorded to concentrations further removed from the interface.

Table 3. Computational Results for Countercurrent Flow
Model No. 2

R	N_x	K_1/K_{F1} Method A	K_1/K_{F1} Method B Phase 1	K_1/K_{F1} Method B Phase 2	Indicated Result
1	200	1.142	1.152	1.148	
	150	1.143	1.156	1.153	
	100	1.145	1.159	1.167	
	50	1.160	1.180	1.190	1.14
2	200	1.115	1.170	1.137	
	150	1.114	1.180	1.145	
	100	1.115	1.198	1.158	
	50	1.124	1.248	1.186	1.12
0.5	200	1.127	1.120	1.142	
	100	1.137	1.124	1.155	
	50	1.156	1.132	1.175	1.116
5	200	1.057	1.280	1.100	
	150	1.054	1.315	1.109	
	100	1.050	1.376	1.124	
	50	1.057	1.531	1.155	1.07
0.2	100	1.098	1.0695	1.148	
	50	1.119	1.0711	1.187	1.066
10	200	1.024	1.541	1.078	
	100	1.018	1.763	1.101	
	50	1.020	2.090	1.133	1.04
0.1	100	1.074	1.0385	1.210	
	50	1.094	1.0380	1.299	1.040
20	200	1.005	2.117	1.063	
	100	0.998	2.586	1.087	
	50	0.999	3.262	1.120	1.02
0.05	100	1.058	1.0194	1.390	
	50	1.079	1.0180	1.585	1.022
50	100	0.982	5.104	1.077	
	50	0.985	6.830	1.110	(1.01)

Table 3. (cont'd)

		$-K_1/K_{F1}$			
			Method B		Indicated
R	N_χ	Method A	Phase 1	Phase 2	Result
0.02	100	1.048	1.0068	1.985	
	50	1.068	1.0049	2.504	1.011
100	100	0.978	9.321	1.074	
	50	0.979	12.794	1.107	(1.005)
0.01	100	1.045	1.0023	2.997	
	50	1.066	1.0002	4.057	1.005

In all cases $\beta = 0.250$

NOMENCLATURE

		Units
a	Proportionality constant in Eqs. (3) and (4), $= 0.343\ u_B \sqrt{u_B/\nu}$	
b	Constant in equilibrium expression Eq. (2).	moles/L^3
$C(\chi,y)_{1,2}$	Local solute concentration in Phases 1 and 2, respectively.	moles/L^3
$D_{1,2}$	Solute diffusivity in Phases 1 and 2, respectively	L^2/T
$k_{1,2}$	Individual local mass transfer coefficient for Phases 1 and 2, respectively. Defined as flux of mass across interface (moles/L^2T) per unit driving force, where driving force is $(C_{1i}-C_{1B})$ for Phase 1 and $(C_{2B}-C_{2i})$ for Phase 2.	$\frac{\text{Moles}/L^2}{T\ \text{Moles}/L^3}$
$k_{1,2}^*$	Average mass transfer coefficient for Phase 1 (or 2) measured in the absence or suppression of resistance in Phase 2 (or 1).	L/T
K_1	Overall mass transfer coefficient based upon driving force $(C_{2Be}-C_{1B})$	L/T
K_{F1}	Value of K_1 predicted by Eq. (1).	L/T
L	Length of exposure interval	L
m	Slope of equilibrium curve, $\left(\frac{dC_{1e}}{dC_2}\right)$. See Eq. (2).	
N_χ	Number of increments considered in χ direction for numerical solution.	
R	mk_1^*/k_2^*. Ratio of individual phase resistances measured independently.	
u	Local velocity in the χ-direction	L/T
v	Local velocity in the y-direction	L/T
$\chi_{1,2}$	Distance away from phase inlet, parallel to interface.	L
$\Delta\chi$	Increment in χ-direction, $= L/N_\chi$	L
$y_{1,2}$	Distance from interface in normal direction	L
$\Delta y_{1,2}$	Increment in y-direction	L

β	Calculational modulus for numerical solution, defined by Eq. (A-6)	
γ	Calculational modulus for Model 2 numerical solution, representing effect of v component of velocity	
δ	Calculational modulus for Model 2 numerical solution, representing effect of u component of velocity.	
ν_2	Kinematic viscosity of Phase 2 fluid	L^2/T

Subscripts

B	Refers to property in bulk fluid, well removed from interface
e	Concentration of indicated phase in equilibrium with the prevailing concentration in the bulk of the other phase
i	Interfacial
X	Local, at a given point of interface
1	Refers to Phase 1
2	Refers to Phase 2

FOOTNOTE AND REFERENCES

*Work performed under the auspices of the U. S. Atomic Energy Commission.

1. Beek, W. J. and C. A. P. Bakker, Appl. Sci. Res., A10, 241 (1961).

2. Carslaw, H. S. and J. C. Jaeger, Conduction of Heat in Solids, 2nd. ed., Oxford (1959). p.63.

3. Emmert, R. E., Ph.D. thesis in Chemical Engineering, University of Delaware (1954).

4. Harriott, P., Can. J. Chem. Eng., 40, 60 (1962).

5. Hildebrand, F. B., Intro. to Numerical Analysis, McGraw-Hill, New York (1956). p. 82.

6. King, C. J., "The Additivity of Individual Phase Resistances in Mass Transfer Operations," paper presented at A.E. Ch. E. Pittsburgh meeting May, 1964. A. I. Ch. E. Jour; to be publ. (1964).

7. Lapidus, L., Digital Computation for Chemical Engineers, McGraw-Hill, New York (1962). Chapter 4.

8. Lightfoot, E. N., A. E. Ch. E. Jour; 8, 416 (1962).

9. Marshall, W. R. and R. L. Pigford, The Application of Differential Equations to Chemical Engineering Problems, Univ. of Delaware, Newark (1947), p. 134.

10. Perlmutter, D. D., Chem. Eng. Sci., 16, 287 (1961).

11. Potter, O. E., Chem. Eng. Sci., 6, 170 (1957).

12. Salvetti, O. and C. Trevessoi, Ann. Chim. (Rome), 51, 207 (1961).

Table 4. FORTRAN program for Model 1 calculations using forward difference solution.

Table V

```
FRDDIF
C       FORWARD DIFFERENCE, DISCARD NET
        READ INPUT TAPE 2,11,NRUNST
   11 FORMAT (I3)
        NRUNS=0
   12 NRUNS=NRUNS+1
        READ INPUT TAPE 2,13,R,BETA,EALL,NX,NTRLM,INT,CONV
   13 FORMAT (3F8.0,3I4,F8.0)
      ODIMENSION C01(1002),C11(1002),C02(1002),C12(1002),CP(1004),CN(1004
      1)
        DIMENSION CF1(1004),CF2(1004)
      ODIMENSION C21(1002),C31(1002),C41(1002),C22(1002),C32(1002),C42(10
      102)
        NXP1=NX+1
        NXP2=NX+2
        XNP2=NXP2
        BNX=NX
        IF (INT) 600,600,599
  599 GO TO (15,17,301,503),INT
   15 DO 16 J=2,NXP2
   16 C01(J)=1000.0
        GO TO 18
   17 DO 19 J=2,NXP2
        BJM2=J-2
   19 C01(J)=1000.0/BNX*BJM2
        GO TO 18
  301 READ INPUT TAPE 2,302,SA,SB,SC,SD
  302 FORMAT (4F8.0)
        DO 303 J=2,NXP2
        BJM2=J-2
  303 C01(J)=1000.0/BNX*BJM2+SA*(SINF(6.2832*BJM2/BNX))+SB*(SINF(4.0*3.1
      1416*BJM2/BNX))+SC*(SINF(8.0*3.1416*BJM2/BNX))+SD*(SINF(16.0*3.1416
      2*BJM2/BNX))
        GO TO 18
  503 READ INPUT TAPE 2,504,PA,PB,PC,PD
  504 FORMAT (4F8.0)
        DO 505 J=2,NXP2
        BJM2=J-2
  505 C01(J)=PA*BJM2/BNX+PB*SQRTF(BJM2/BNX)+PC*BJM2/BNX*BJM2/BNX+PD*(BJM
      12/BNX)**10
        GO TO 18
C       INITIAL ESTIMATE OF INTERFACIAL CONCENTRATION PROFILE
  600 DO 716 J=3,NXP1
        BJ=J
        FJ=(XNP2-BJ)/(BJ-2.0)
  716 C01(J)=1000.0/(1.0+R*SQRTF(FJ))
        DO 717 I=3,NXP1
        JSUB=NX+4-I
  717 C02(I)=C01(JSUB)
        C01(NXP2)=1000.0
```

```
FRODIF
      C02(NXP2)=0.0
      C02(2)=1000.0
      C01(2)=0.0
      NTRLS=1
   18 FCTR=(1.0-2.0*BETA)
      DO 8 I=1,NXP2
      C11(I)=0.0
      C21(I)=0.0
      C31(I)=0.0
      C41(I)=0.0
    8 CN(I)=C.0
      CN(2)=BETA*C01(2)
      C11 (3)=CN(2)
      DO 20 I=1,NXP2
   20 CP(I)=C.0
      N=2
      DO 23 J=4,NXP2
      CP(1)=C01(J-1)
      DO 21 I=2,N
   21 CP(I)=CN(I)
      IF (CN(N)-0.1) 900,900,901
  901 N=N+1
  900 DO 22 I=2,N
   22 CN(I)=BETA*(CP(I-1)+CP(I+1))+FCTR*CP(I)
      C21(J)=CN(3)
      C31(J)=CN(4)
      C41(J)=CN(5)
   23 C11(J)=CN(2)
      CN(1)=1000.0
      DO 29 I=N,NXP2
   29 CN(I)=0.0
      DO 730 I=1,NXP2
  730 CF1(I)=CN(I)
      IF (INT) 740,740,41
  740 N=2
      DO 9 I=1,NXP2
      C12(I)=1000.0
      C22(I)=1000.0
      C32(I)=1000.0
      C42(I)=1000.0
    9 CN(I)=1000.0
      CN(2)=BETA*C02(2)+(1.0-BETA)*1000.0
      C12(3)=CN(2)
      DO 24 I=1,NXP2
   24 CP(I)=1000.0
      DO 27 J=4,NXP2
      CP(1)=C02(J-1)
      DO 25 I=2,N
   25 CP(I)=CN(I)
      IF (999.90-CN(N)) 902,902,903
```

```
FRDDIF
  903 N=N+1
  902 DO 26 I=2,N
   26 CN(I)=BETA*(CP(I-1)+CP(I+1))+FCTR*CP(I)
      C22(J)=CN(3)
      C32(J)=CN(4)
      C42(J)=CN(5)
   27 C12(J)=CN(2)
      CN(1)=C.0
      DO 28 I=N,NXP2
   28 CN(I)=1000.0
      DO 731 I=1,NXP2
  731 CF2(I)=CN(I)
C     CONVERGENCE PROCEDURE
   31 NADJ=0
      DO 33 J=3,NXP1
      ISUB=NX+4-J
      ERR=ABSF((-(25.0*C01(J)-48.0*C12(ISUB)+36.0*C22(ISUB)-16.0*C32(ISU
     1B)+3.0*C42(ISUB))/(25.0*C01(J)-48.0*C11(J)+36.0*C21(J)-16.0*C31(J)
     2+3.0*C41(J))-R)/R)
      IF (ERR-EALL) 33,33,32
   32 NADJ=NADJ+1
      CIND=(48.0*C12(ISUB)-36.0*C22(ISUB)+16.0*C32(ISUB)-3.0*C42(ISUB)+R
     1*(48.0*C11(J)-36.0*C21(J)+16.0*C31(J)-3.0*C41(J)))/(25.0*(R+1.0))
      CNEW=C01(J)+CONV*(CIND-C01(J))
      C01(J)=CNEW
      C02(ISUB)=C01(J)
   33 CONTINUE
      WRITE OUTPUT TAPE 3,34,NADJ
   34 FORMAT (6H NADJ=I3)
      WRITE OUTPUT TAPE 3,7,CF2(2),CF1(2)
    7 FORMAT (3H CF2(2)= F10.5/8H CF1(2)= F10.5)
      IF (NADJ-5) 41,41,35
   35 NTRLS=NTRLS+1
      IF (NTRLS-21) 37,36,37
   36 GO TO (40,37,37),NTRLM
   37 IF (NTRLS-41) 39,38,39
   38 GO TO (40,40,39),NTRLM
   39 GO TO 18
   40 GO TO 800
C     FINAL INTEGRATIONS
   41 DEL=NX
      DIMENSION RATIOL (999)
      FCT=(SQRTF(3.1416*DEL*BETA))*(1.0+R)/2000.0
      DO 42 I=3,NXP1,1
   42 RATIOL(I-2)=(FCT/12.0)*(25.0*C01(I)-48.0*C11(I)+36.0*C21(I)-16.0*C
     131(I)+3.0*C41(I))
      EVEN=0.0
      ODD=0.0
      NXM2=NX-2
      NXM3=NX-3
```

```
 FRDDIF
      DO 43 K=2,NXM2,2
   43 EVEN=EVEN+RATIOL(K)
      DO 44 K=3,NXM3,2
   44 ODD=ODD+RATIOL(K)
      DEN=NX-2
      RATIOK=(2.0*ODD+4.0*EVEN+RATIOL(1)+RATIOL(NX-1))/(3.0*DEN)
C     TOTAL TRANSFER FROM PHASE ONE
      FCT=(1.0+R)/6000.0*SQRTF(3.1416/(BETA*DEL))
      ODD=0.0
      EVEN=0.0
      DO 45 I=2,NX,2
   45 EVEN=EVEN+CF1(I)
      NXM1=NX-1
      DO 46 I=3,NXM1,2
   46 ODD=ODD+CF1(I)
      TTRNS1=FCT*(4.0*EVEN+2.0*UDD+1000.0+CF1(NXP1))
C     TOTAL TRANSFER FROM PHASE TWO
      IF (INT) 47,47,61
   47 FCT=(1.0+R)/6000.0/R*SQRTF(3.1416/(BETA*DEL))
      ODD=0.0
      EVEN=0.0
      DO 48 J=2,NX,2
   48 EVEN=EVEN+1000.0-CF2(J)
      DO 49 J=3,NXM1,2
   49 ODD=ODD+1000.0-CF2(J)
      TTRNS2=FCT*(4.0*EVEN+2.0*ODD+2000.0-CF2(NXP1))
C     PRINTED OUTPUT AND RETURN TO NEXT RUN
   61 WRITE OUTPUT TAPE 3,62,NRUNS
   62 FORMAT (25H1 OUTPUT FROM RUN NUMBER  I3)
      WRITE OUTPUT TAPE 3,94,R,BETA,EALL,NX,INT,NTRLS
  940FORMAT (3HOR= F10.4/6H BETA= F10.4/6H EALL= F6.5/4H NX= I4/5H INT=
     1 I4/7H NTRLS= I4)
      WRITE OUTPUT TAPE 3,910,CONV
  910 FORMAT (20H CONVERGENCE FACTOR= F10.4)
      IF (INT) 65,65,60
   60 GO TO (65,65,63,69),INT
   63 WRITE OUTPUT TAPE 3,64,SA,SB,SC,SD
   64 FORMAT (4H SA= F10.5/4H SB= F10.5/4H SC= F10.5/4H SD= F10.5)
      GO TO 65
   69 WRITE OUTPUT TAPE 3,70,PA,PB,PC,PD
   70 FORMAT (4H PA= F10.5/4H PB= F10.5/4H PC= F10.5/4H PD= F10.5)
   65 WRITE OUTPUT TAPE 3,66,RATIOK,TTRNS1,TTRNS2
  660FORMAT (38HOK/K FROM INTERFACIAL INTERIOR POINTS= F12.8/ 35H K/KF
     1FROM TOTAL TRANSFER, PHASE 1= F12.8/ 35H K/KF FROM TOTAL TRANSFER,
     2 PHASE 2= F12.8)
      WRITE OUTPUT TAPE 3,67,(RATIOL(I),I=1,NXM1)
   67 FORMAT (44HO LOCAL K/K FOR INTERNAL POINTS OF INTERFACE/(10F11.4))
      WRITE OUTPUT TAPE 3,68,(CF1(I),I=1,NXP1)
   68 FORMAT (29HO EXIT CONCENTRATIONS,PHASE 1/(10F11.4))
      WRITE OUTPUT TAPE 3,71,(CF2(I),I=1,NXP1)
```

```
FRCDIF
   71 FORMAT (29HO EXIT CONCENTRATIONS,PHASE 2/(10F11.4))
      WRITE CUTPUT TAPE 3,92,(C01(J),J=2,NXP2)
   92 FORMAT (28HC INTERFACIAL CONCENTRATIONS/(10F11.4))
  800 IF (NRUNS-NRUNST) 12,91,91
   91 CALL EXIT
      END(1,1,0,0,0,0,1,0,0,1,0,0,0,0,0)
```

Table 5. FORTRAN program for Model 2 calculations using Crank-Nicholson solution.

Table IV

```
BLAYER
C       PHASE 1 PENETRATION, PHASE 2 BOUNDARY LAYER FIRST TERM APPROX.
C       CRANK-NICHOLSON SCHEME, SOLVE BY THOMAS METHOD
C       FIVE POINT APPROXIMATION TO INTERFACIAL FLUXES
        READ INPUT TAPE 2,11,NRUNSI
     11 FORMAT (I3)
        NRUNS=0
     12 NRUNS=NRUNS+1
        READ INPUT TAPE 2,13,R,BETA,EALL,NX,NTRLM,INT,CONV
     13 FORMAT (3F8.0,3I4,F8.0)
        DIMENSION CO1(202),C11(202),CO2(202),C12(202),CP(202),CN(202)
        DIMENSION CF1(204),CF2(204)
        DIMENSION C21(202),C31(202),C41(202),C22(202),C32(202),C42(202)
        NXP1=NX+1
        NXP2=NX+2
        XNP2=NXP2
        BNX=NX
C       INITIAL ESTIMATE OF INTERFACIAL CONCENTRATION PROFILE
    600 DO 716 J=3,NXP1
        BJ=J
        FJ=(XNP2-BJ)/(BJ-2.0)
    716 CO1(J)=1000.0/(1.0+R*SQRTF(FJ))
        DO 717 I=3,NXP1
        JSUB=NX+4-I
    717 CO2(I)=CO1(JSUB)
        CO1(NXP2)=1000.0
        CO2(NXP2)=0.0
        CO2(2)=1000.0
        CO1(2)=0.0
        BETA32=BETA*SQRTF(BETA)
        DIMENSION GAMMA(202,50),DELTA(202,50)
        DO 203 I=3,NXP2
        AI=I
        AIS=SQRTF(AI-2.5)
        DO 203 J=2,50
        BJ=J-1
        DELTA(I,J)=(3.07*BJ)/(BETA32*AIS)
    203 GAMMA(I,J)=DELTA(I,J)*BJ/(16.0*(AI-2.5))
        NTRLS=1
C       PHASE ONE, CRANK-NICHOLSON
        DIMENSION D(52),AJ(52),B(52),E(52),W(52),Q(52),G(52)
     18 A=2.0+2.0/BETA
        FCTR=2.0/BETA-2.0
        DO 19 I=1,NXP2
        C11(I)=0.0
        C21(I)=0.0
        C31(I)=0.0
        C41(I)=0.0
     19 CN(I)=0.0
        CN(2)=CO1(3)/A
```

BLAYER

```
      C11(3)=CN(2)
      DO 20 I=1,NXP2
   20 CP(I)=0.0
      N=3
      DO 23 J=4,NXP2
      CP(1)=C01(J-1)
      DO 21 I=2,N
   21 CP(I)=CN(I)
  901 IF (N-49) 905,900,900
  905 N=N+1
  900 D(2)=C01(J)+C01(J-1)+CP(3)+FCTR*CP(2)
      DO 22 I=3,N
   22 D(I)=CP(I-1)+CP(I+1)+FCTR*CP(I)
      G(2)=D(2)/A
      W(2)=A
      DO 24 K=3,N
   24 W(K)=A-1.0/W(K-1)
      DO 25 L=3,N
   25 G(L)=(D(L)+G(L-1))/W(L)
      CN(N)=G(N)
      NM1=N-1
      DO 26 I=2,NM1
      ISUB=N+1-I
   26 CN(ISUB)=G(ISUB)+CN(ISUB+1)/W(ISUB)
      C21(J)=CN(3)
      C31(J)=CN(4)
      C41(J)=CN(5)
   23 C11(J)=CN(2)
      CN(1)=1000.0
      DO 29 I=N,NXP2
   29 CN(I)=0.0
      DO 730 I=1,NXP2
  730 CF1(I)=CN(I)
C     PHASE TWO, BOUNDARY LAYER, CRANK-NICHOLSON
      N=3
      DO 201 I=1,NXP2
      C12(I)=1000.0
      C22(I)=1000.0
      C32(I)=1000.0
      C42(I)=1000.0
  201 CN(I)=1000.0
     OCN(2)=((1.0+GAMMA(3,2))*C02(3)+((1.0-GAMMA(3,2)+DELTA(3,2))*1000.0
     1))/(DELTA(3,2)+2.0)
      C12(3)=CN(2)
      DO 204 I=1,NXP2
  204 CP(I)=1000.0
      DO 205 J=4,NXP2
      CP(1)=C02(J-1)
      DO 206 I=2,N
  206 CP(I)=CN(I)
```

```
BLAYER
 904 IF (N-49) 903,902,902
 903 N=N+1
 902CD(2)=(1.0+GAMMA(J,2))*(CO2(J-1)+CO2(J))+(DELTA(J,2)-2.0)*CP(2)+(1.
    10-GAMMA(J,2))*CP(3)
     DO 207 I=3,N
 207CD(I)=(1.0+GAMMA(J,I))*CP(I-1)+(DELTA(J,I)-2.0)*CP(I)+(1.0-GAMMA(J,
    1I))*CP(I+1)
     CD(N)=(1.0+GAMMA(J,N))*CP(N-1)+(DELTA(J,N)-2.0)*CP(N)+2000.0*(1.0-G
    1AMMA(J,N))
     DO 208 K=2,N
 208 AJ(K)=DELTA(J,K)+2.0
     DO 209 L=3,N
     B(L-1)=GAMMA(J,L-1)-1.0
 209 E(L)=-(1.0+GAMMA(J,L))
     W(2)=AJ(2)
     DO 210 K=3,N
     Q(K-1)=B(K-1)/W(K-1)
 210 W(K)=AJ(K)-E(K)*Q(K-1)
     G(2)=D(2)/W(2)
     DO 211 L=3,N
 211 G(L)=(D(L)-E(L)*G(L-1))/W(L)
     CN(N)=G(N)
     NM1=N-1
     DO 212 I=2,NM1
     ISUB=N+1-I
 212 CN(ISUB)=G(ISUB)-CN(ISUB+1)*Q(ISUB)
     C22(J)=CN(3)
     C32(J)=CN(4)
     C42(J)=CN(5)
 205 C12(J)=CN(2)
     CN(1)=0.0
     DO 213 I=N,NXP2
 213 CN(I)=1000.0
     DO 731 I=1,NXP2
 731 CF2(I)=CN(I)
     CONVERGENCE PROCEDURE
  31 NADJ=0
     DO 33 J=3,NXP1
     ISUB=NX+4-J
    0ERR=ABSF((-(25.0*C01(J)-48.0*C12(ISUB)+36.0*C22(ISUB)-16.0*C32(ISU
    1B)+3.0*C42(ISUB))/(25.0*C01(J)-48.0*C11(J)+36.0*C21(J)-16.0*C31(J)
    2+3.0*C41(J))-R)/R)
     IF (ERR-EALL) 33,33,32
  32 NADJ=NADJ+1
    0CIND=(48.0*C12(ISUB)-36.0*C22(ISUB)+16.0*C32(ISUB)-3.0*C42(ISUB)+R
    1*(48.0*C11(J)-36.0*C21(J)+16.0*C31(J)-3.0*C41(J)))/(25.0*(R+1.0))
     CNEW=CO1(J)+CONV*(CIND-CO1(J))
     CO1(J)=CNEW
     CO2(ISUB)=CO1(J)
  33 CONTINUE
```

```
BLAYER

      WRITE OUTPUT TAPE 3,34,NADJ
   34 FORMAT (6H NADJ=I3)
      WRITE OUTPUT TAPE 3,7,CF2(2),CF1(2)
    7 FORMAT (8H CF2(2)= F10.5/8H CF1(2)= F10.5)
      IF (NADJ-5) 41,41,35
   35 NTRLS=NTRLS+1
      IF (NTRLS-61) 37,36,37
   36 GO TO (40,37,37),NTRLM
   37 IF (NTRLS-41) 39,38,39
   38 GO TO (40,40,39),NTRLM
   39 GO TO 18
   40 GO TO 800
C     FINAL INTEGRATIONS
   41 DEL=NX
      DIMENSION RATIOL (199)
      FCT=(SQRTF(3.1416*DEL*BETA))*(1.0+R)/2000.0
      DO 42 I=3,NXP1,1
   42 RATIOL(I-2)=(FCT/12.0)*(25.0*C01(I)-48.0*C11(I)+36.0*C21(I)-16.0*C
     131(I)+3.0*C41(I))
      EVEN=0.0
      ODD=0.0
      NXM2=NX-2
      NXM3=NX-3
      DO 43 K=2,NXM2,2
   43 EVEN=EVEN+RATIOL(K)
      DO 44 K=3,NXM3,2
   44 ODD=ODD+RATIOL(K)
      DEN=NX-2
      RATIOK=(2.0*ODD+4.0*EVEN+RATIOL(1)+RATIOL(NX-1))/(3.0*DEN)
C     TOTAL TRANSFER FROM PHASE ONE
      FCT=(1.0+R)/6000.0*SQRTF(3.1416/(BETA*DEL))
      ODD=0.0
      EVEN=0.0
      DO 45 I=2,NX,2
   45 EVEN=EVEN+CF1(I)
      NXM1=NX-1
      DO 46 I=3,NXM1,2
   46 ODD=ODD+CF1(I)
      TTRNS1=FCT*(4.0*EVEN+2.0*ODD+1000.0+CF1(NXP1))
C     TOTAL TRANSFER FROM PHASE TWO
      FCT=(1.0+R)/(2200.0*R*BETA*DEL)
      ODD=0.0
      EVEN=0.0
      DO 214 J=2,NX,2
      WGT=J-1
  214 EVEN=EVEN+WGT*(1000.0-CF2(J))
      DO 215 J=3,NXM1,2
      WGT=J-1
  215 ODD=ODD+WGT*(1000.0-CF2(J))
      TTRNS2=FCT*(4.0*EVEN+2.0*ODD)
```

```
BLAYER
C       PRINTED OUTPUT AND RETURN TO NEXT RUN
   61 WRITE OUTPUT TAPE 3,62,NRUNS
   62 FORMAT (25H1 OUTPUT FROM RUN NUMBER  I3)
      WRITE OUTPUT TAPE 3,94,R,BETA,EALL,NX,INT,NTRLS
   94 FORMAT (3HOR= F10.4/6H BETA= F10.4/6H EALL= F6.5/4H NX= I4/5H INT=
     1 I4/7H NTRLS= I4)
      WRITE OUTPUT TAPE 3,910,CONV
  910 FORMAT (20H CONVERGENCE FACTOR= F10.4)
   65 WRITE OUTPUT TAPE 3,66,RATIOK,TTRNS1,TTRNS2
   66 FORMAT (38HOK/K FROM INTERFACIAL INTERIOR POINTS= F12.8/ 35H K/KF
     1FROM TOTAL TRANSFER, PHASE 1= F12.8/ 35H K/KF FROM TOTAL TRANSFER,
     2 PHASE 2= F12.8)
      WRITE OUTPUT TAPE 3,67,(RATIOL(I),I=1,NXM1)
   67 FORMAT (44HO LOCAL K/K FOR INTERNAL POINTS OF INTERFACE/(10F11.4))
      WRITE OUTPUT TAPE 3,68,(CF1(I),I=1,NXP1)
   68 FORMAT (29HO EXIT CONCENTRATIONS,PHASE 1/(10F11.4))
      WRITE OUTPUT TAPE 3,71,(CF2(I),I=1,NXP1)
   71 FORMAT (29HO EXIT CONCENTRATIONS,PHASE 2/(10F11.4))
      WRITE OUTPUT TAPE 3,92,(CO1(J),J=2,NXP2)
   92 FORMAT (28HO INTERFACIAL CONCENTRATIONS/(10F11.4))
  800 IF (NRUNS-NRUNST) 12,91,91
   91 CALL EXIT
      END(1,1,0,0,0,0,1,0,0,1,0,0,0,0,0)
```

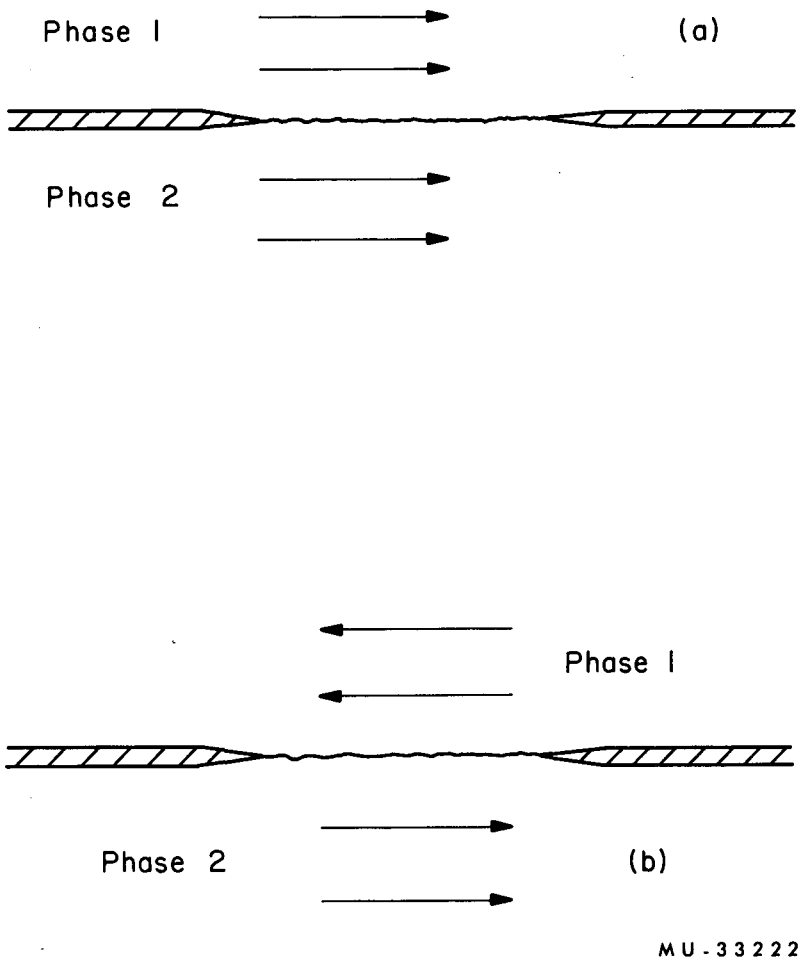

Fig. 1. (a) Cocurrent exposure; (b) countercurrent exposure.

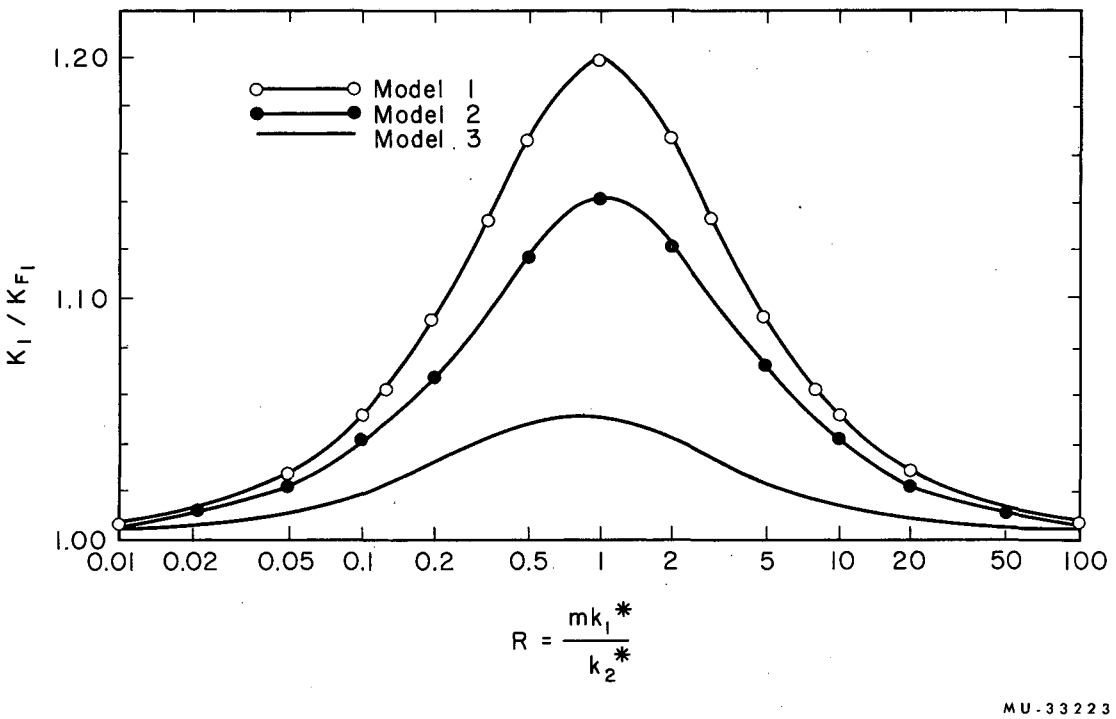

Fig. 2. Over-all mass transfer coefficients - deviation from Eq. (1).

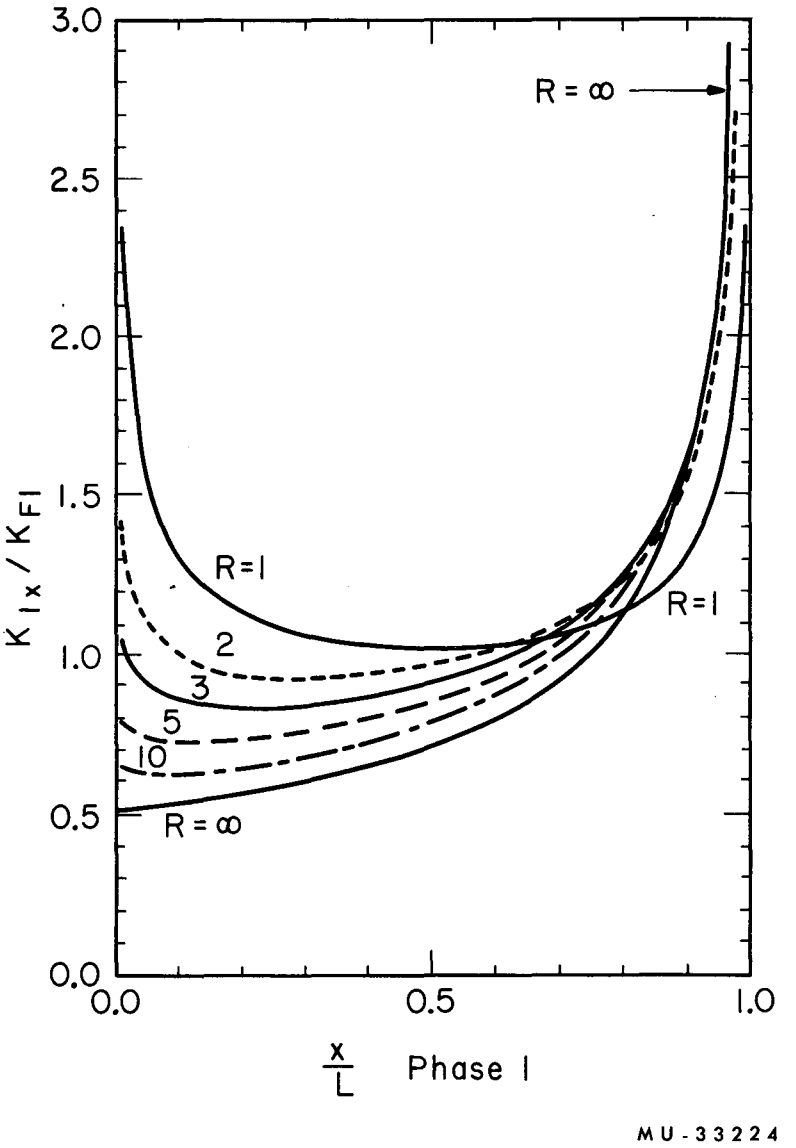

Fig. 3. Local mass transfer rates, Model 1.

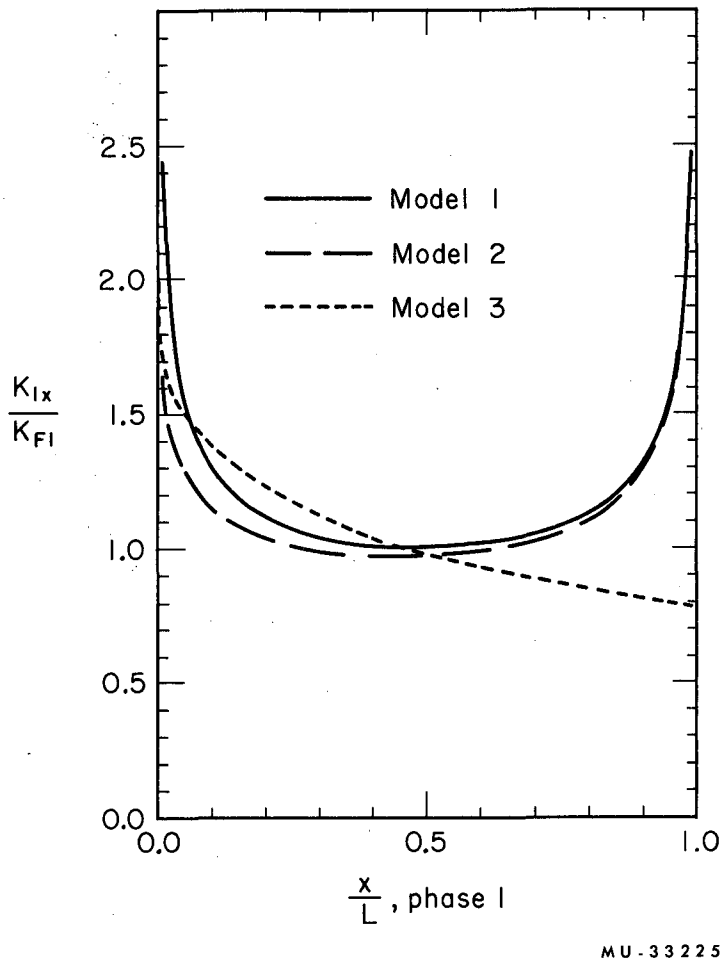

Fig. 4. Local mass transfer rates; comparison of models. R = 1.

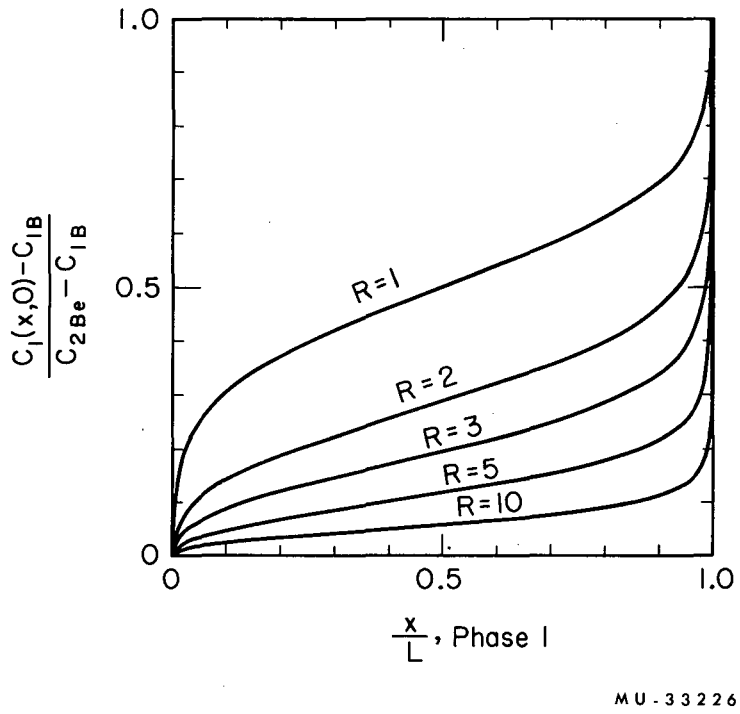

Fig. 5. Interfacial concentrations, Model 1.

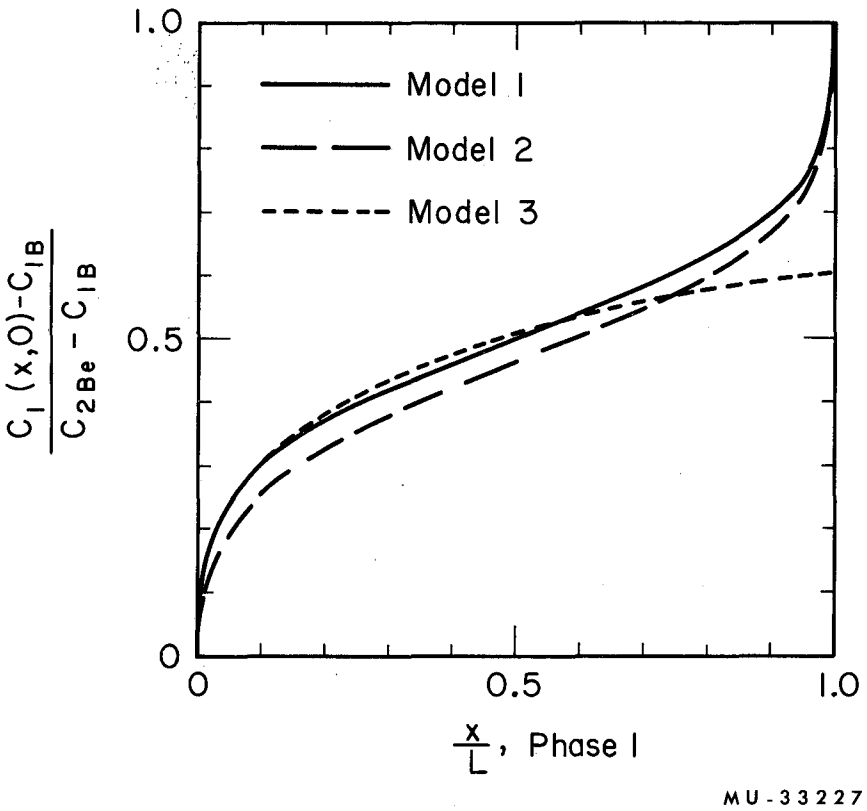

Fig. 6. Interfacial concentrations; comparison of models. R = 1.

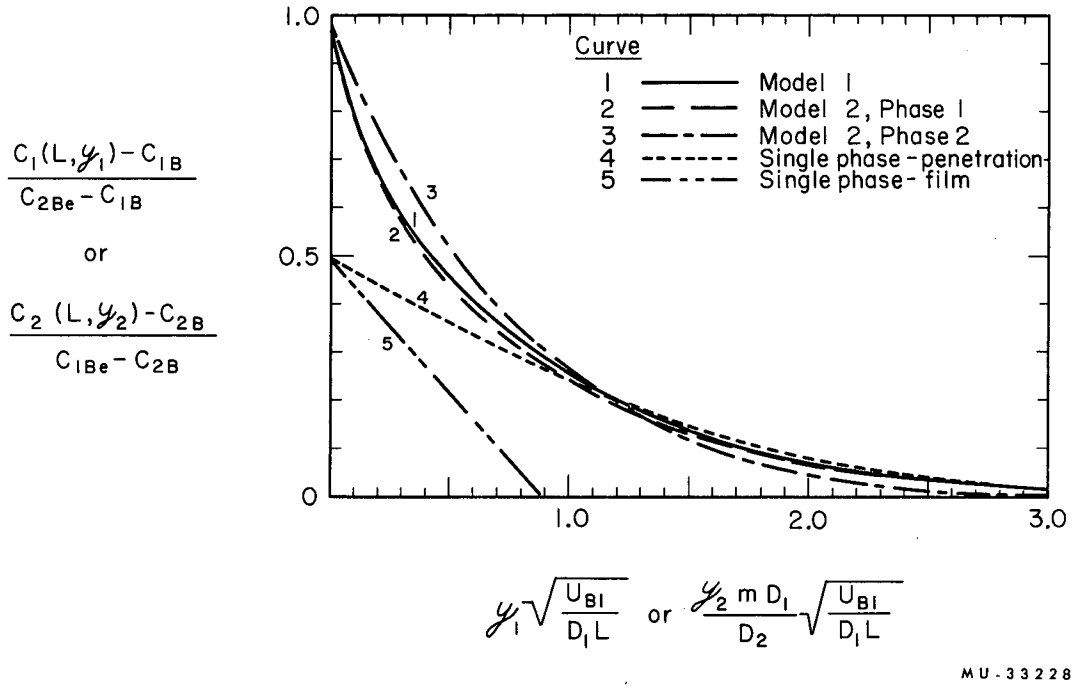

Fig. 7. Effluent concentrations; comparison of models. R = 1.